# Influence of nonradiative Auger process in the lanthanide complexes lifetime near interfaces in organic light-emitting diode structures

Cite as: J. Appl. Phys. **126**, 165501 (2019); doi: 10.1063/1.5099014 Submitted: 5 April 2019 · Accepted: 29 September 2019 · Published Online: 22 October 2019







Alessandra Pereira,<sup>1,2,a)</sup> Gilmar Conte,<sup>3</sup> Angelo D. Faceto,<sup>4</sup> D Luis A. O. Nunes,<sup>4</sup> Welber G. Quirino,<sup>5</sup> Cristiano Legnani,<sup>5</sup> D Hugo Gallardo,<sup>3</sup> D Marco Cremona,<sup>1</sup> D Ivan H. Bechtold,<sup>6</sup> D and Francisco E. G. Guimarães<sup>4,b)</sup>

# **AFFILIATIONS**

a) Email: ales\_p18@yahoo.com.br, Tel.: +55 24 22311542.b) Email: guimarae@ifsc.usp.br, Tel.: +55 16 33739792.

# **ABSTRACT**

The low efficiency of organic light-emitting diodes based on lanthanide complexes is generally attributed to the triplet-triplet annihilation processes in the regime of high concentration of excited states caused by their long lifetimes and optical losses near the interfaces of multilayer device structures. Despite the enormous effort to synthesize short-lived complexes and minimize the optical losses in the interfaces, it remains insufficient in understanding the exciton recombination processes that reduce the lifetime of these complexes. Herein, we investigated the influence of the exciton recombination processes on a Tb complex (Tb-C) lifetime in the regime of a highly excited state concentration as a function of the distance between the carrier layer and the interface by using a typical organic light-emitting diode structure. Our results show that a 10 nm-thick Alq<sub>3</sub> layer decreases the exciton lifetime of the Tb-C, increasing approximately by 16 times the spontaneous emission decay rate of triplet exciton. The effects of interference and optical losses at the metallic interface contribute actively to the modulation of the emission intensity and lifetime decay. However, these effects alone do not explain the significant increase in the emission decay rate. The nonradiative Auger process at the Alq<sub>3</sub>/Tb-C interface seems to be largely accountable for the Tb-C lifetime reduction as the energy released by the terbium ion occurs by the excitation of an adjacent electron at higher energy. Furthermore, we propose a simple theoretical model to explain the observed effects. These results can provide a new approach to reduce the lanthanide complexes' lifetime through the Auger electron process near the interface and thus improve the performance of organic light-emitting diodes.

Published under license by AIP Publishing. https://doi.org/10.1063/1.5099014

#### I. INTRODUCTION

Organic light-emitting diodes (OLEDs) are among the technologies that dominate the market for mobile devices and displays. The development of new classes of organic compounds, novel approaches to device structures, and efficient methods to improve their efficiency are the main factors for their success.<sup>1</sup>

However, the fabrication of full-color OLED based displays still has some challenges, such as the poor color purity due to the intrinsic nature of broad emission spectra of the fluorescent organic molecules, phosphorescent organic-metal complexes, and thermally activated delayed fluorescence (TADF) organic molecules used widely as emitters in this kind of devices.<sup>2–4</sup>

Department of Physics, Pontifical Catholic University of Rio de Janeiro, Rio de Janeiro, 22451-900, RJ, Brazil

<sup>&</sup>lt;sup>2</sup>Division of Metrology of Materials, National Institute of Metrology, Standardization and Industrial Quality (INMETRO), Duque de Caxias, 252250-020, RJ, Brazil

<sup>&</sup>lt;sup>3</sup>Department of Chemistry, Federal University of Santa Catarina, Florianópolis, 88040-900, SC, Brazil

São Carlos Institute of Physics, University of São Paulo, São Carlos, 13560-970, SP, Brazil

<sup>&</sup>lt;sup>5</sup>Department of Physics, Federal University of Juiz de Fora, Juiz de Fora, 36036-900, MG, Brazil

<sup>&</sup>lt;sup>6</sup>Department of Physics, Federal University of Santa Catarina, Florianópolis, 88040-900, SC, Brazil

In the last three decades, lanthanide complexes have appeared as possible emitter alternatives due to their unique properties, such as sharp emission bands (nearly monochromatic emission), compared to other organic emitters.  $^{5,6}$  However, the device performance based on these complexes is still unsatisfactory when compared to that of devices using pure organic or phosphorescent compounds as emitters. The device efficiency drops rapidly by increasing the current density in lanthanide-based OLEDs. Extensive research suggests that this roll-off efficiency is due to the long luminescence lifetimes of the emitters and triplet-triplet (T-T) and triplet-polaron (P-T) annihilations.  $^{7,8}$  Recently, Su *et al.* reported a new organoeuropium complex with a short lifetime of  $30\,\mu s$ . Their results demonstrated that the emitter's short luminescence lifetime reduced the efficiency roll-off for the fabricated OLEDs. Nevertheless, the devices' current efficiency reached a maximum of 3.0 cd/A at 10 V.

Furthermore, the lanthanide complexes and other organic emitters have their luminescence lifetime changed near the interfaces present in the devices. 10,11 In fact, metallic and dielectric interfaces provide additional optical paths that can produce changes in the spontaneous molecular emission with significant modifications in the spectrum of the emitted light. As the dimensions of such devices are typically on the scale of one-half of the optical wavelengths or less of the emitter material, the presence of nearby interfaces may control the emission behavior of the molecules and, consequently, plays a vital role in the device performance. Kowalsky et al. 12 observed a significant improvement in the electroluminescence (EL) quantum efficiency of their europium based OLEDs at a high current density using a microcavity device. Samuel et al. 13 demonstrated a powerful approach to modulate the light emission and its propagation by the use of photonic microstructures using solvent assisted microcontact molding (SAMIM) in increasing the efficiency of the solutionprocessed europium based OLEDs through efficient light extraction from the substrate mode. Thereafter, many improvements in the OLED performance and optical outcoupling have been where different metal structures and materials have been used to achieve better reflectivity and radiative quantum efficiency. Thus, understanding the modulation of the lifetime of lanthanide complexes near the interfaces of devices is essential to reduce the roll-off efficiency to improve the efficiency of the OLEDs based on lanthanide complexes.

In the OLED structure, in addition to the dielectric and metallic interfaces, different functional organic layers forming organic heterojunctions are also present. In the case of a significant energy barrier at the organic heterojunctions, charges will accumulate at the respective interfaces, resulting in the formation of charge transfer (CT) excitons between two adjacent layers. The Auger process is the typical formation of nonradiative charge transfer (CT) excitons. <sup>17</sup> For organic semiconductors, the Auger electron process may involve bimolecular recombination, where the energy released from the interface charge transfer exciton recombination is transferred to excite another electron into higher-energy states (Auger electron). Lu et al. 18 fabricated ultralow-voltage OLEDs with device structures using stimulated Auger electrons. In this case, the nonradiative Auger process plays a crucial role in the attainment of ultralow voltage, also increasing the OLED efficiency. In other words, using OLED structures that favor the Auger processes, it is possible to modulate the lanthanide complexes' lifetime. Besides, it can support an ultralow-voltage OLED based on Auger electron injection.

In our work, we investigated the influence of the charge transfer (CT) exciton recombination at the organic heterojunctions and metallic or dielectric interfaces on the spontaneous emission rate and the lifetime of a Tb complex probe layer inserted in a typical multilayer OLED structure. The Tb complex is the ([1,2,5]thiadiazolo[3,4-f][1,10]phenanthroline)Tb(acetylacetonate-ACAC)<sub>3</sub>]), also indicated as [Tb(ACAC)<sub>3</sub>TDZP] or simply Tb-C. To evaluate the electrode's (ITO or Al) influence on the emitting layer, we fabricated two structures: ITO/HTL/EL (where HTL is the hole transporting layer) and EL/ETL/Al (where ETL is the electron transporting layer), which were studied separately. In particular, the luminescence properties of thin Tb-C layers were studied as a function of their distance from the Al and ITO electrodes using Alq<sub>3</sub> [(tris(8-hydroxyquinoline)aluminum(III)] and NPB [(N,Ń-bis(naphthalene-1-y)-N, Ń-bis(phenyl)benzidine)] as organic spacers with thicknesses of 0-20 nm.

#### **II. MATERIALS AND METHODS**

Figure 1 shows the vacuum-processed stack structure OLEDs [Fig. 1(a)], molecular structures of the compounds [Fig. 1(b)], and the energy level diagrams [Fig. 1(c)]. The glass and ITO/glass patterned substrates were sequentially sonicated for 10 min at 75 °C in a detergent solution [5 wt. % of Extran in de-ionized (DI) water], DI water, acetone, and 2-propanol. After, the substrates have been dried with nitrogen gas, followed by UV-ozone treatment for 30 min to adjust the work function and improve the wetting. All of the layers were sequentially deposited by thermal evaporation under high vacuum (≈10<sup>-6</sup> Pa) and without exposure to the atmosphere. We fabricated two device structures, stack structures I and II, containing 7 or 40 nm, respectively, of a Tb-C film as the emitter layer. Stack structure I consisted of a glass substrate partially covered with 150 nm of Al and 0-20 nm of Alq3 as an electron transporting layer (ETL). The active Tb-C layer was deposited sequentially onto Alq3. Stack structure II consisted of a patterned ITO/glass with 0-20 nm of the NPB film as the hole transporting layer (HTL) and the Tb-C film on top. These transporting layers were called the "spacer layers." The stack structures had their thicknesses measured by a Dektak 6M profilometer.

The luminescent properties of the Tb-C active layer in both structures were studied using photoluminescence (PL) and continuous wave (CW) time-resolved luminescence spectroscopy. The room temperature photoluminescence and excitation spectra of the Tb-C and the corresponding laser excitation wavelengths used in the present work are shown for comparison in Fig. S1 (see the supplementary material). The PL spectra were recorded using an HR4000 Ocean Optics spectrometer as a detection system. The active layer was excited through the glass on different structure configurations [the black arrows in Fig. 1(a) represent 325 nm and 442 nm HeCd laser lines with an average excitation intensity of 5 nW/cm<sup>2</sup>]. The measurement was performed via a backscattering configuration in two ways: in the first, the Tb-C active layer was excited from the Al and from the ITO for stack structures I and II, respectively; in the second configuration, the uncoated glass of structures I and II had the active layer probed

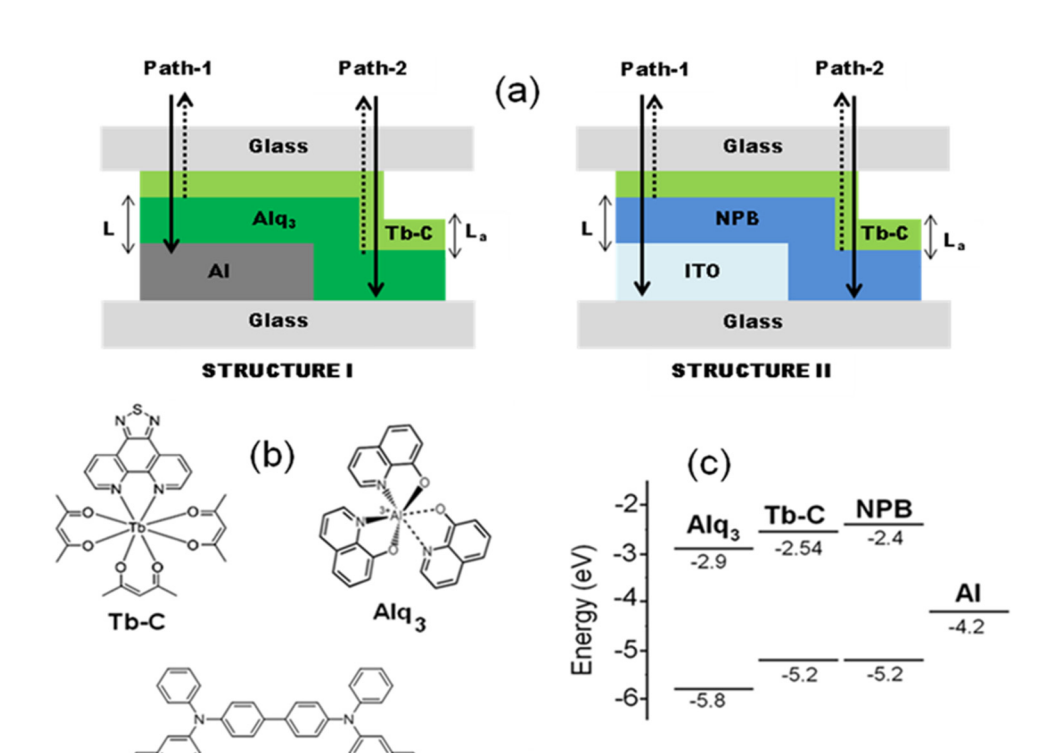
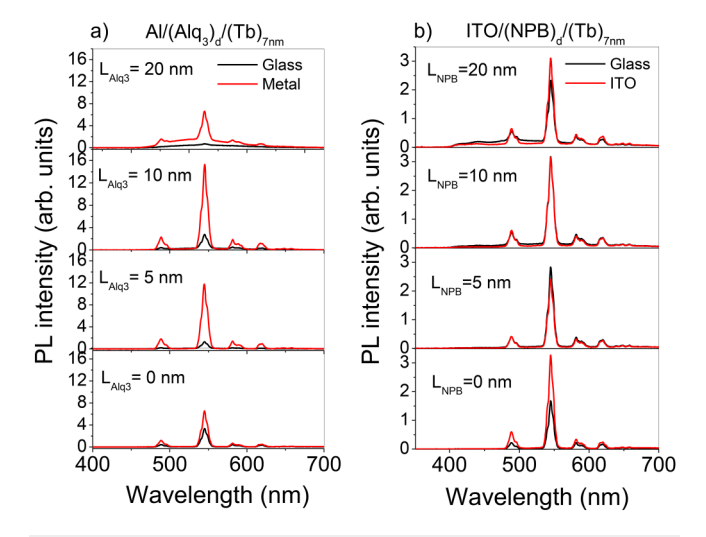


FIG. 1. (a) Representation scheme of the vacuum-processed stack structures I and II. The arrows represent the excitation (solid arrows) and emission (dashed arrows) wavelengths; (b) the chemical structures of the materials and (c) the rigid band diagram with the relative positions of the LUMO and HOMO levels of the organic layers.

[Figure 1(a)]. The dashed arrows in Fig. 1(a) indicate the Tb-C optical emission. The PL spectra were measured as a function of the spacer thickness on the metal in structure I and on the ITO in structure II. We denominate the luminescence signal measured on the ITO-uncoated and Al-uncoated glass substrates as reference samples. During the PL measurements, the optical path of the

NPB



**FIG. 2**. The PL of the 7 nm probe Tb-C layer as a function of the  $Alq_3$  and NPB spacer thickness L in structure I (a) and structure II (b), respectively.

exciting and emitted light remained fixed. All of the measures were conducted at room temperature and in an ambient atmosphere.

The luminescence decay was detected using a Thermo Jarrell Ash monochromator (25 cm focal length) equipped with a Hamamatsu R298 photomultiplier tube. A digital oscilloscope processed the signal averaging over 250 pulses. Time-resolved measurements were conducted using a pulsed  $N_2$  laser at 337 nm.

# **III. RESULTS AND DISCUSSION**

A thin Tb-C layer (7 nm) was used to probe the optical properties of the interfaces for structures I and II. In particular, we investigate the excited state dynamics of the Tb-C layer as a function of its distance from the Al and ITO electrodes. Figures 2(a) and 2(b) compare the PL of the Tb-C probe layer for structure I (glass/Alq<sub>3</sub>/Tb-C) and structure II (ITO/NPB/Tb-C) as a function of Alq<sub>3</sub> and NPB thicknesses (L), respectively. In structure I [Fig. 2(a)], the decrease in the PL intensity for the Tb-C layer deposited onto the Alq<sub>3</sub> spacer compared to the Tb-C film deposited onto the plain glass surfaces (black lines) indicates that the charge or energy transfer was expected from the rigid energy band diagram [Fig. 1(c)]. However, the samples prepared on the Al metal-coated surfaces and depending on the Alq<sub>3</sub> spacer thickness L present a strong enhancement in the Tb-C emission.

For structure II [Fig. 2(b)], the intensity of the Tb-C emission is almost the same for all of the spacer thicknesses  $(0 \le L \le 20)$  measured on the reference sample and the ITO surfaces. This behavior indicates that there is no loss in the excited state at the ITO anode when L=0. Furthermore, no energy

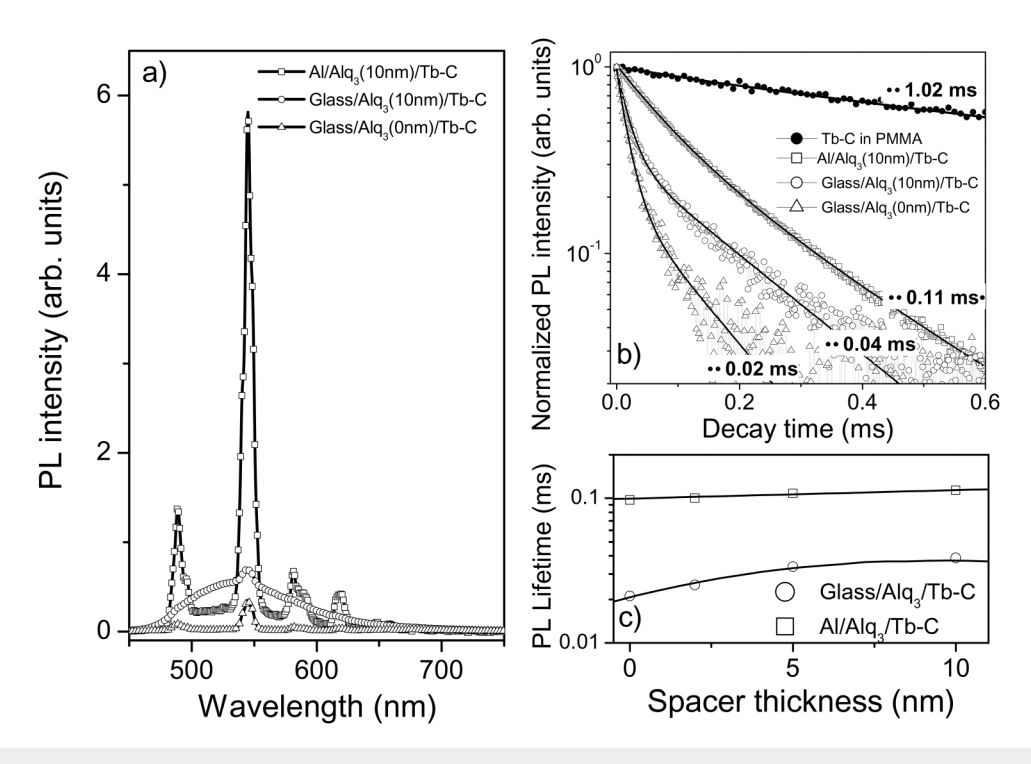


FIG. 3. The PL emission and dynamics of a Tb-C layer for structure I. (a) the PL spectra measured at 300 K; (b) the PL decays of the Tb-C for the three cases shown in (a); and (c) the PL decay times for the same 40 nm-thick Tb-C layers deposited onto the glass reference and Al surfaces as a function of the Alq<sub>3</sub> spacer thickness.

charge transfer takes place from the Tb-C ligand to the NPB when L>0.

Figure 3 shows the effect of the interfaces on the PL emission and dynamics for structure I with a thick Tb-C layer (40 nm). Figure 3(a) compares the PL spectrum of the Tb-C layer deposited directly onto the glass (open triangles) with that of the same Tb-C deposited onto the Al cathode spaced with a 10 nm Alq<sub>3</sub> film (open squares). In this case, the emission of the Tb-C is approximately 16 times more intense than for the same film measured directly on the glass reference surface (open triangles). The broad Alq<sub>3</sub> emission band also appears superimposed to the Tb-C spectrum due to the excitation wavelength (325 nm) used in the experiment. The intensity of the Alq3 band demonstrates a significant reduction when deposited onto the Al surface due to charge/energy transfer losses to the metallic electrode. Also, only a weak signal from the Tb-C layer is detected when it is deposited directly onto the glass (open triangles) or when it is separated from the glass by the Alq<sub>3</sub> spacer (open circles).

The different behaviors of the luminescence previously presented can be better understood with time-resolved photoluminescence measurements. Figure 3(b) compares the PL decays of the 546 nm emission line of Tb-C for the three cases shown in Fig. 3(a), excited by the 337 nm line of a pulsed  $N_2$  laser. For comparison purposes, we used the PL decay of Tb-C embedded in a PMMA matrix (closed circles). Here, we expect to observe the decay properties of noninteracting complex molecules due to their substantial dilution in the PMMA matrix. Furthermore, the Alq $_3$  fast emission

decay (nanoseconds) is not detected in the millisecond time scale presented in Fig. 3(b). The same happens for the laser pulse with a width of 5 ns.

Since the decay patterns involve a complex interplay between different effects that complicate a theoretical analysis, we analyze the PL decay evolution of the Tb-C within the framework of a stretched exponential  $I(t) = I_0 \exp[-(t/\tau)^{\beta}]^{19}$  In this equation,  $\tau$ represents an active PL decay time and  $\beta$  introduces the stretch coefficient. The coefficient  $\beta$  varies between 0 and 1, where its value represents the multiplicity of concurrent processes that deactivate the Tb radiative channel for decay times in the range of microseconds to milliseconds. A single exponential decay  $(\beta \sim 1)$ within  $\tau$  = 1.02 ms was found for the Tb-C isolated in the PMMA matrix corresponding roughly to the natural lifetime  $\tau_0$  of the isolated Tb ions. This scenario changes dramatically for the 40 nm-thick Tb-C films deposited onto different surfaces. The mean decay time  $\tau$  sharply decreases to 0.02 ms in the Tb-C layers evaporated directly on the glass surface (open triangles) but doubles to 0.04 ms with the inclusion of a 10 nm-thick Alq<sub>3</sub> spacer between the Tb-C active layer and the glass surface (open circles). The decay time  $\tau$  increases further to approximately 0.11 ms when the same layer structure is excited on the Al surface (open

Table I summarizes the PL decay times  $\tau$  as well as the corresponding  $\beta$  values, the estimated PL decay rates  $(K = \frac{1}{\tau} = k_R + k_{RN})$ , and the PL quantum yields  $\eta = \frac{k_R}{K}$  for structure I with an Alq<sub>3</sub>

**TABLE I.** The PL decay times  $\tau$ , the estimated PL decay rates  $(K = \frac{1}{\tau} = k_R + k_{RN})$ , and the estimated values for the  $\beta$  and PL quantum yields  $\eta = \frac{k_R}{2\tau}$  for structures I and II.

Sample	τ (ms)	$K(s^{-1})$	β	$\eta \ (k_R = 1000 \ \text{s}^{-1}) \ (\%)$
Glass/Tb-C	0.02	50 000	0.54	2
Glass/Alq3/Tb-C	0.04	23 255	0.57	4.3
Al/Alq3/Tb-C	0.18	5 555	0.80	18
Tb-PMMA	1	1 000	1	100

layer thickness of 10 nm, as shown in Fig. 3(b). Here,  $k_R = \frac{1}{r_0}$  is the natural radiative decay rate of the isolated Tb-C, which was assumed to be  $1000~\rm s^{-1}$ , and  $k_{RN}$  takes into account all concurrent nonradiative decay rates. It is important to stress that only optical processes occurring close the Tb natural decay rate  $k_R$  were considered in this evaluation of the radiative quantum yield. In this work, concurrent nonradiative processes faster than  $1/\rm s$  were not detected.

The progressive increase in the  $\beta$  coefficient from 0.54 for the glass reference interface to 0.80 for the metallic interface (see Table I) indicates that part of the processes competing for radiation has been "turned off" with the introduction of the spacer layer and the metal surface. This effect reflects a decrease in the total decay rate k and a sequential increase in the emission efficiency  $\eta$ . Compared to the Tb-C deposited directly onto the glass surface ( $\beta$  = 0.54,  $k \sim 5.0 \times 10^4 \, \rm s^{-1}$ ), the turning-off of the deactivation process is more expressive for the Tb-C deposited onto the Al surface ( $\beta$  = 0.80,  $k \sim 5.5 \times 10^3 \, \rm s^{-1}$ ) than that observed for the same layer structure on the nearby glass surface ( $\beta$  = 0.57,  $k \sim 23 \times 10^3 \, \rm s^{-1}$ ).

The enhancement in the PL intensities shown in Fig. 3(a) can be attributed to the increase in the emission quantum yield ( $I_{PL}$ ) presented in Table I. Concerning the glass/Tb-C reference sample, the efficiency  $\eta$  of the Tb-C layer enhances by a factor of only 2 with the introduction of the Alq<sub>3</sub> spacer layer on the glass surface and a factor of almost 9 when it is onto the Al surface. However, a best-fitting procedure of the PL spectra in Fig. 3(a) reveals that Tb-C emission intensity increases at least 16 times for the Al/Alq<sub>3</sub>/Tb-C sample in comparison with the emission intensity of the glass/Tb-C reference sample.

The introduction of the reflecting metal interface necessarily includes interference effects that would increase the PL intensity by a maximum factor of 4, depending on the distance and the orientation of the molecule emitter concerning the metallic mirror. Moreover, an excited molecule or a rare-earth ion near to a metallic interface suffers modification in the decay time. 20 According to Drexhage and Jose,<sup>21</sup> the radiative decay rate of a europium complex oscillates around its natural value depending on the distance to the metallic interface, but these variations would not exceed a factor of 2. For an excited emitter positioned at intervals below 5 nm from a metallic interface, the decay rate would increase drastically due to the loss of energy to surface plasmons via rapid nonradiative charge transfer processes.<sup>22</sup> These changes depend on the reflectivity of the metal surface. However, both the interference effects and modification of decay times introduced by the metallic interfaces are insufficient to explain the significant increase of 16 times observed for the PL intensity, as mentioned earlier.

To obtain better insights into the different effects that interfaces impose on the recombination processes in the Tb-C active layer, Fig. 3(c) displays the PL decay times for the same 40 nm-thick Tb-C layers deposited onto the glass and Al surfaces as a function of the Alq<sub>3</sub> spacer thickness. The PL decay time  $\tau$ increases by approximately a factor of 2 (open circles) with the spacer thickness for the glass surface, but this behavior eventually saturates for the spacer thickness greater than 10 nm. For samples onto the Al surface (open squares),  $\tau$  is 4–5 times higher than reference samples. However, its dependence on the spacer thickness is virtually negligible. The variation in  $\tau$  for the reference samples is an indication that the Alq<sub>3</sub> layer acts as a buffer layer that isolates the substrate effects in the film, which is probably caused by the charged radicals on the glass surface. As discussed below, these contradictory findings would be suitably explained by the excited state dynamics in disordered materials with long decay times, such as the Tb-C.

The different values of the PL decay behavior and the amplification observed in the case of the Al surface were not found for the corresponding 40 nm-thick Tb-C layers in structure II deposited directly onto the ITO. Figure 4 summarizes the interface effects in the PL spectra (a) and decays (b) measured at 300 K for the glass surface (squares, assumed as reference) or separated by the 10 nm NPB spacer layers from the glass (triangles) and the ITO surfaces (circles). The Tb-C spectrum is superimposed onto the broad NPB emission with the maximum at 435 nm when we used the 325 nm excitation line of a He-Cd laser [Fig. 4(a)]. The Tb-C emission component presents no enhancement but falls within the inclusion of the spacer layer due to the partial absorption of the excitation light by the NPB, as was observed for the Alq<sub>3</sub> spacer. Figure 4(b) compares the PL decay of the samples presented in Fig. 4(a) with that of the Tb-C embedded in a PMMA matrix (closed circles). The excitation and optical paths were the same as those used in Fig. 3 for structure I. For structure II, the decay behavior for the Tb-C is almost the same, independent if the NPB spacer layer is onto the reference sample or the ITO surfaces. The mean PL decay time of approximately 0.02 ms was evaluated for all of the samples as expected. Interestingly, the NPB does not act as a buffer layer as was observed for the Alq<sub>3</sub> spacer.

The dependence of the Tb-C emission on the spacer thickness L, as shown in Fig. 3, can be followed in Fig. 5(a). This behavior can be plotted as a function of the intensity ratios between the luminescence intensities measured on the Al-coated ( $I_{\rm Al}$ ) and ITO ( $I_{\rm ITO}$ ) surfaces and the reference intensity measured on the glass ( $I_{Glass}$ ) surface. Thus, this figure compares the intensity ratios  $I_{\rm Al}/I_{\rm Glass}$ (structure I) and  $I_{\rm ITO}/I_{\rm Glass}$  (structure II) for Tb-C layer thicknesses of 7 nm (stars) and 40 nm (circles) as a function of the respective  $Alq_3$  and NPB thicknesses. The value of the  $I_{ITO}/I_{Glass}$  ratio is approximately equal to 1 for all of the NPB spacer thicknesses and both Tb-C layers. However, for the Al surface, the  $I_{\rm Al}/I_{\rm Glass}$  ratio strongly depends on both the Alq<sub>3</sub> spacer and Tb-C thickness (closed stars and circles). As the PL intensity on the glass surface,  $I_{\text{Glass}}$  is practically constant (see Fig. 3), the variation in the  $I_{\text{Al}}/I_{\text{Glass}}$ ratio depends only on the PL intensity  $I_{Al}$  recorded for the Al surface. In this case, the  $I_{\rm Al}/I_{\rm Glass}$  ratio consistently varies up to 50 times (10 times) with the spacer layer thickness L in the range of 0-20 nm for the 40 nm Tb-C emitting layer (7 nm). For the

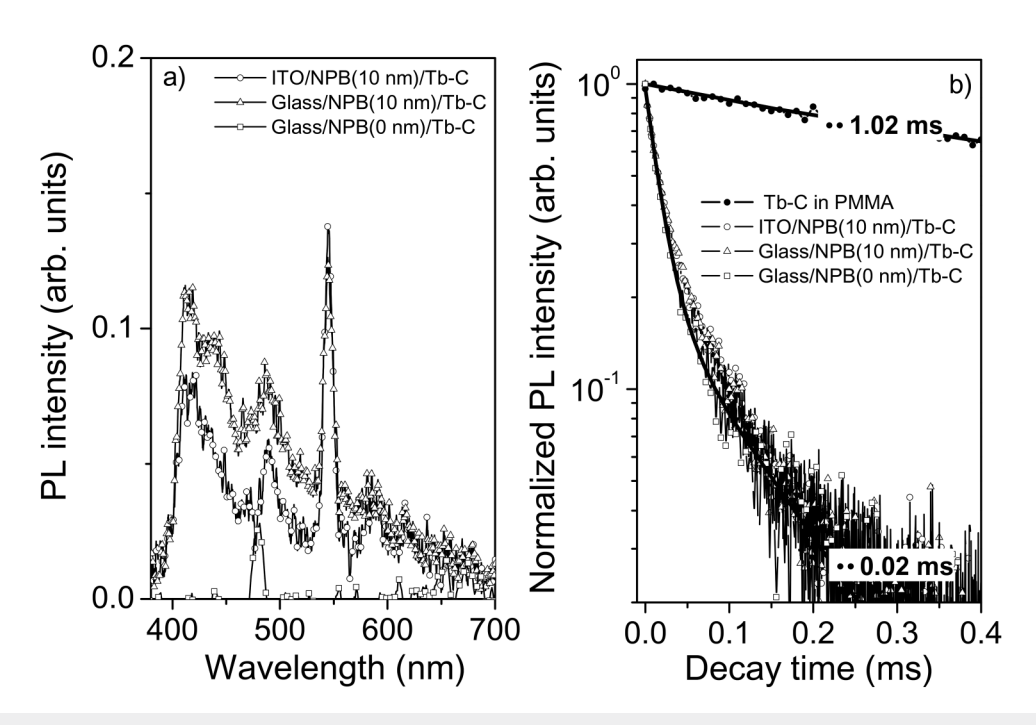


FIG. 4. The PL spectra (a) and decay (b) measured at 300 K for the glass surface as the reference (squares) or separated by the 10 nm-thick NPB spacer from the glass (triangles) and ITO surfaces (circles).

7-nm-thick Tb-C layer, the intensity shrinks when the separation between the metal surface and the Tb-C layer is smaller than 5 nm, which is associated with losses due to the charge and energy transfer to the metal. In the 40 nm-thick Tb-C layer, this annihilation effect may be suppressed by the emitting centers present within the layer and far from the metallic interface.

Figure 5(a) also includes the theoretically calculated intensity ratios (solid lines) of structures I and II as a function of the separation L between the Al surface and the 7 nm and 40 nm active emissive layers. The calculation takes into account two effects: (1) the eventual losses due to the charge/energy transfer from an excited Tb-C molecule to the collective excitations in the metal or (2) the interference between the emitted radiation of the Tb-C molecule propagating outside the sample and the counterpropagating radiation reflected by the metallic surface.

Considering the contribution of a single Tb-C molecule in the emitting layer as an oscillating dipole at a distance L from the metallic interface, an approximate theoretical value for I (L)/ $I_0$  can be calculated according to the approach of Deppe  $et\ al.^{23}$  (see the supplementary material). The interaction length  $L_0=5$  nm for the charge/energy transfer processes was estimated from Fig. 5(c), which shows the emission intensity of the Alq<sub>3</sub> spacer layer in structure I, measured on the metallic surface and the glass surface as a function of its thickness. The Alq<sub>3</sub> emission on the glass surface linearly increases with its thickness as expected. For the metallic surface, the intensity of the same layer remains very low up to 5 nm and increases similar to that of the glass surface for higher layer thicknesses. This behavior of the excited state,

generated within a spacer layer of 5 nm, migrates to the metallic interface, and there it is deactivated through the charge/energy transfer processes. This range of interaction was also reported by Borges *et al.*,<sup>24</sup> for similar structures based on a very thin poly (1,4-phenylene vinylene) (PPV) emitting layer prepared using the layer-by-layer (LbL) technique.

The emission profile for a single molecule near a metallic plane, as shown in Fig. 5(b), does not fit the experimental data of Fig. 5(a) for the  $I_{Al}/I_{Glass}$  intensity ratio. In Fig. 5(b), horizontal bars represent the integration intervals. These bars were scaled and displaced according to the two Tb-C layer thicknesses of 7 nm (short white bars) and 40 nm (long gray bars) and the thickness of the Alq<sub>3</sub> spacer layer, respectively. As depicted in Fig. 5(a), both calculated intensity ratios were corrected equally by a factor of 2.5 to obtain the corresponding intensity ratios. The factor of 2.5 corresponds to the theoretical adjustment for the calculated intensity profile  $I(L)/I_0$  relation of the Tb-C emitter as a function of the spacer layer (L) at the metallic interface. The reduction for the 7 nm Tb-C sample when compared to the 40 nm Tb-C sample can be explained by the fact that a part of the total electronic energy of the Tb-C molecule can be transferred or migrated to vibrational modes during the emission due to the conformational change of the molecule during emission decay of the excited state to the ground state. The relative intensity between them depends on the value of the electron-phonon coupling. There are, therefore, many details of the sample structure that influence the form and efficiency of the active layer emission intensity with the distance from a metal-covered surface.

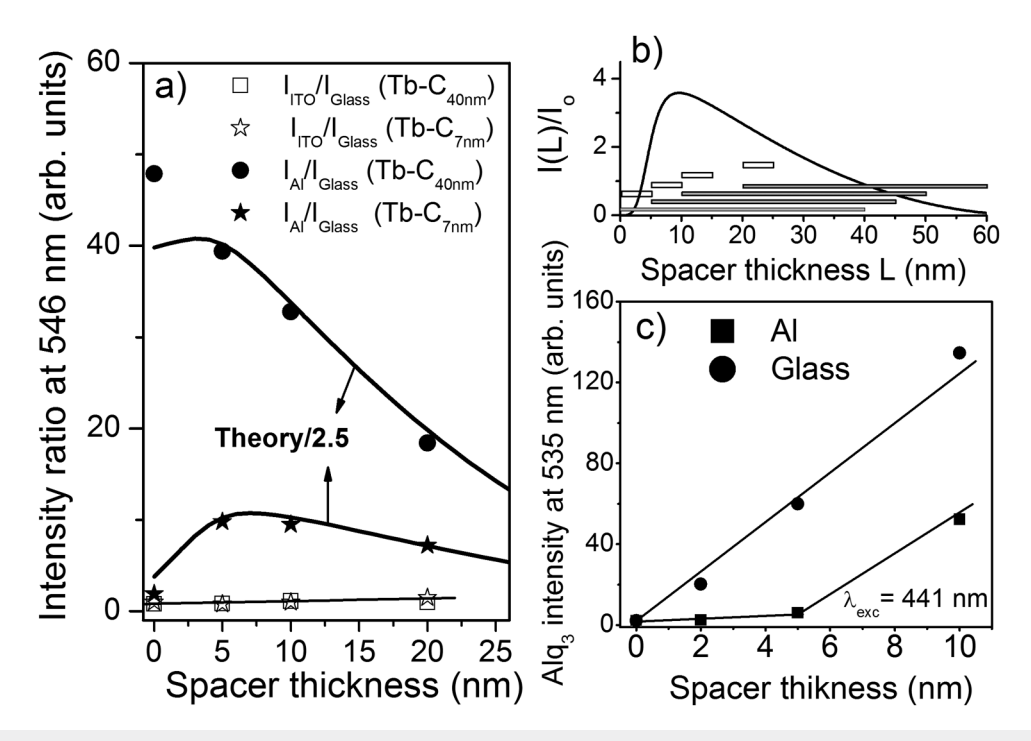


FIG. 5. (a) The theoretically calculated intensity ratios (solid lines) for structures I and II as a function of the separation L between the AI surface and the active emissive layer; (b) the calculated intensity profile I (L)/I<sub>0</sub> for a single dipole parallel to 150 nm-thick AI (the horizontal bars correspond to the integration range); and (c) the estimated interaction length.

The relatively small modulation of the Tb natural lifetime induced by the metal at the interface produces additional behavior that weakly affects the final dependence on the spacer thickness as depicted in Fig. 5(a). However, the significant expressive increase in the quantum efficiency by a factor of 9 for the Tb-C deposited onto metallic surfaces could never be achieved by modifications of the natural decay rate induced by the metallic interface. The changes in the decay rates could be more readily associated with the optical processes in the samples. The significant increase in the decay rate k from  $1000 \, \text{s}^{-1}$  for the Tb-C in the PMMA matrix to  $50\,000 \, \text{s}^{-1}$  for the evaporated Tb-C layer on the glass or ITO surfaces can be associated mainly with the elimination of nonradiative channels that rapidly decrease the Tb-C excitation state in a dense solid-state film. Also, these nonradiative processes occur for elapsed times that fall in the decay range of microseconds to milliseconds in our measurements.

Consequently, rapid charge and/or energy transfer processes that would quench the emission are rolled out in the present sample structures. However, an effective energy homotransfer process between the Tb-C molecules would be sufficient to promote the incoherent migration of the excited state and guide this molecular excitation to quenching centers inside the active layer. In solid films, the excitation can migrate over much larger distances (~10 nm) than the few nanometers established by the Förster radius (~1–2 nm for heterotransfer between donors and acceptors). Therefore, any nonradioactive channel that deactivates the Tb-C excited state would act for times close to the Tb lifetime if the migration of the excited state continues to proceed until the final emission process.

Migration is very effective between high energy levels within the density of state (DOS) distribution of high density. The Tb-C ligands would promote migration via energy transfer between high energy states. The migration would be strongly reduced after the rapid spectral relaxation of a few picoseconds to low-density tail states at the bottom of the DOS. This process is due to the electronic relaxation via spectral diffusion.<sup>25</sup> However, the low lying states are those belonging to the long-lived Tb ions. As there is one Tb ion per complex, the bottom of the DOS consists of high density isoenergetic Tb3+ states that actively promote migration via energy transfer processes. The time needed to reach the lower-lying equilibrium energy is much shorter for Tb-C than its intrinsic lifetime. Although migration proceeds after electronic relaxation due to thermal activation, the diffusivity of the excited state decreases since the number of target sites, including the quenching centers, reached during migration substantially decreases. One of the main deactivation mechanisms in evaporated Tb-C films of high molecular density is the effective migration of the excited state via Förster-type energy transfer processes (homotransfers) between Tb-C molecules that could end up at quenching centers. However, these processes are rapid (< nanoseconds) and could not be detected in the decay ranges used in the present work.

Radiationless transfer processes should not be influenced by the presence of interfaces<sup>26</sup> unless the transfer rate  $k_T = 1/\tau$  (R<sub>o</sub>/R)<sup>6</sup> is modified by the change in the excited state decay rate  $k = 1/\tau$  of the donor molecule. R<sub>o</sub> and R are the Förster critical radius and the distance between the two interacting molecular dipoles,

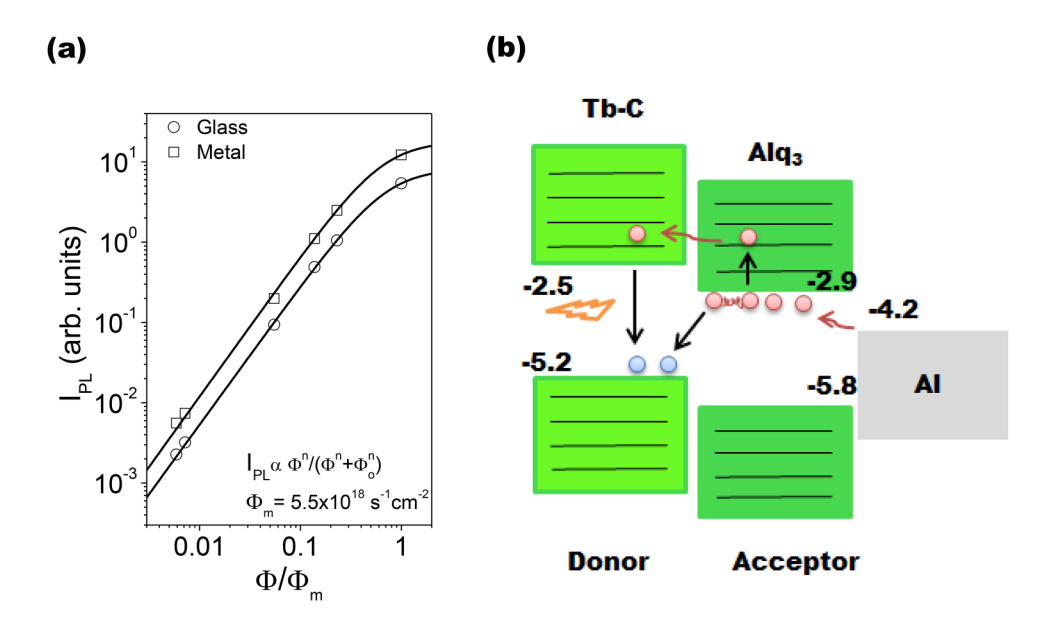


**FIG. 6.** (a) The PL intensities measured for the Tb-C emission at 546 nm in structure I as a function of the laser fluence  $\Phi$  normalized by the maximally adjusted fluence  $\Phi_m$  and (b) schematic diagram of an Auger process at the organic semiconductor heterojunction Tb-C/Alq<sub>3</sub>.

respectively. Metallic and dielectric interfaces may directly alter the lifetime of an excited molecule due to the change in the boundary conditions of the electromagnetic fields of the emitted light. The emission lifetime would be lengthened or shortened depending on the distance of the luminescent molecule from the interface. A reduction k would increase  $k_T$  and  $k_{NR}$ .

Increasing the pump levels could progressively enhance the annihilation processes that lead to Tb-C emission saturation for higher pump fluences due to efficient Auger annihilation processes. Figure 6(a) compares the PL intensities measured for the Tb-C emission at 546 nm for structure I considering the metal and glass interfaces as a function of the laser fluence  $\Phi$  normalized by the maximally adjusted fluence  $\Phi_{\mathrm{m}}$ . This pump power dependence can be readily fitted to the universal behavior  $I_{PL} \propto \left[\frac{\Phi^n}{(\Phi^n + \Phi_0^n)}\right]$ , where  $\Phi_0 = 1/\sigma\tau$  is the flux necessary for the formation of two nearby excitons at different Tb-C molecules with cross sections of  $\sigma$  during the natural exciton lifetime  $\tau$ . The exponent n defines the characteristics of the recombination process (mono- or bimolecular).  $I_{PL}$ increases linearly for the regime of low pump intensity  $(\Phi < \Phi_0)$  with an angular coefficient n = 7/4 for both samples and saturates at higher pump values  $(\Phi > \Phi_0)$  due to the effective nonradioactive Auger decay channel. The fitting procedure is  $\Phi_0 \sim 3.7 \times 10^{18} \, \text{s}^{-1} \, \text{cm}^{-2}$ , which results in the value for the absorption cross section  $\sigma$  for the Tb-C of approximately  $2.7 \times 10^{-16}$  cm<sup>2</sup>, assuming a natural lifetime  $\tau$  for isolated Tb ions of 1 ms [Fig. 3(b)], which is close to the typical crosssectional value for most organic dyes (10<sup>-16</sup> cm<sup>2</sup>).<sup>27</sup> Furthermore, the similar fitting values found for  $\Phi_0$  indicate that the natural lifetime of Tb ions is not expressively modified by the presence of the metallic interface compared to the reference glass interface. Therefore, the short decay times visible in Figures 4 and 5 and measured for the Tb-C were strictly produced by non-radioactive Auger processes since pump fluencies of  $\Phi = 5.5 \times 10^{18} \ s^{-1} \ cm^{-2}$  are higher than the one used in the time decay measurements.

Note, however, that the interference effects and losses of energy to surface plasmons via rapid nonradiative charge transfer processes are not enough to explain the 16 times increase in the PL emission of Tb-C observed in Fig. 3(a). Therefore, our results suggest three different physical pathways for charge transfer exciton recombination at structure I: (i) interference effects that would increase the PL intensity by a maximum factor of 4, depending on the distance and the orientation of the molecule emitter concerning the metallic mirror; 14,21 (ii) energy transfer near the interface, where a Dexter or a Förster process is responsible for transferring the energy of the charge transfer excitons to another acceptor molecule. For an excited emitter positioned at intervals below 5 nm from a metallic interface, the decay rate would increase drastically due to the loss of energy to surface plasmons via rapid nonradiative charge transfer processes;<sup>22</sup> (iii) an Auger process at the Tb-C/Alq<sub>3</sub> interface. Figure 6(b) shows the schematic diagram of an Auger process at the organic semiconductor heterojunction Tb-C/Alq3, where the energy of a third particle (electron or hole) is shaken up by nonradiative recombination of the charge transfer excitons. Owing to the large energy offsets on both the HOMOs and LUMOs, electrons and holes accumulate at the Tb-C/Alq<sub>3</sub> interface, leading to an Auger recombination. The Auger process involving valence shells (conduction band to valence band) is typically a lowprobability event. However, previous works<sup>27,28</sup> suggest that the 4d-4f direct recombination occurs in the lanthanide complex is associated with a coupled Auger process. In an Auger electron process, one electron from the LUMO of the electron transport

layer (ETL) recombines with one hole from the HOMO of Tb-C by exciting another electron on the Alq<sub>3</sub> LUMO to a higher energy level (Auger electron). This Auger electron will then be the resonant level between the Alq<sub>3</sub> triplet state around  $2.17 \pm 0.5 \, \text{eV}^{2.9}$  and the  $^5D_4 \rightarrow ^7F_4$  transition of Tb<sup>+3</sup> ion with triplet state at 2.12 eV (583 nm).

#### IV. CONCLUSIONS

Our results demonstrate that metallic interface effects directly affect the emission dynamics of the active layer in OLEDs. In particular, the experiments conducted using the Tb(ACAC)<sub>3</sub>TDZP terbium complex (Tb-C) as an active layer showed that a metallic Al interface substantially enhances the Tb-C emission. Also, there are many details on the sample structure that influences the form and efficiency of the emission intensity of the active layer with the distance from a metal-covered surface. The effects of interference and optical losses at the metallic interface contribute actively to the modulation of the emission intensity and lifetime decay. However, only these effects are insufficient for the significant increase in the emission decay rate. The nonradiative Auger process at the Alq<sub>3</sub>/Tb-C interface seems to be the foremost accountable for the Tb-C lifetime reduction as the energy released by the terbium ion occurs by excitation of an adjacent electron at higher energy. Finally, this study presented and discussed theoretical models that thoroughly explain the observed effects, which can be generally applied to elucidate quenching mechanisms of emitting species close to metallic interfaces.

# SUPPLEMENTARY MATERIAL

See the supplementary material for optical characterizations of the organic materials and theoretical model details.

#### **ACKNOWLEDGMENTS**

The authors acknowledge the financial support of INCT/INEO, CNPq, FAPERJ, and CAPES.

#### **REFERENCES**

<sup>1</sup>C. W. Han and Y. H. Tak, in *Flat Panel Display Manufacturing*, edited by Jun Souk, Shinji Morozumi, Fang-Chen Luo, and Ion Bita (John Wiley & Sons Ltd, 2018), p. 143.

- <sup>2</sup>Z. Yang, Z. Mao, Z. Xie, Y. Zhang, S. Liu, J. Zhao, J. Xu, Z. Chi, and M. P. Aldred, Chem. Soc. Rev. 46, 915 (2017).
- <sup>3</sup>H. Jeong, H. Shin, J. Lee, B. Kim, Y.-I. Park, K. S. Yook, B.-K. An, and J. Park, J. Photonics Energy 5, 057608 (2015).
- <sup>4</sup>H. Sasabe and J. Kido, Eur. J. Org. Chem. 2013 7653 (2013).
- <sup>5</sup>C. Wei, L. Ma, H. B. Wei, Z. W. Liu, Z. Q. Bian, and C. H. Huang, Sci. China Technol. Sci. **61**, 1265 (2018).
- <sup>6</sup>E. Girotto, A. Pereira, C. Arantes, M. Cremona, A. J. Bortoluzzi, C. A. M. Salla, I. H. Bechtold, and H. Gallardo, J. Lumin. **208**, 57 (2019).
- <sup>7</sup>T. W. Canzler and J. Kido, Org. Electron. Phys. Mater. Appl. 7, 29 (2006).
- <sup>8</sup>J. Mezyk, D. Di Nuzzo, A. Mech, R. Tubino, and F. Meinardi, J. Chem. Phys. 132, 024504 (2010).
- <sup>9</sup>L. Zhang, B. Li, L. Zhang, and Z. Su, ACS Appl. Mater. Interfaces 1, 1852 (2009).
- 10K. H. Drexhage and S. Jose, J. Luminescence 2, 693 (1970).
- <sup>11</sup>R. Ranjan, E. N. Esimbekova, M. A. Kirillova, and V. A. Kratasyuk, Anal. Chim. Acta 971, 1 (2017).
- <sup>12</sup>S. Dirr, S. Wiese, H.-H. Johannes, D. Ammermann, A. Böhler, W. Grahn, and W. Kowalsky, Synth. Met. 91, 53 (1997).
- 13S. Zhang, G. A. Turnbull, and I. D. W. Samuel, Appl. Phys. Lett. 103, 10 (2013).
- <sup>14</sup>C. Murawski, P. Liehm, K. Leo, and M. C. Gather, Adv. Funct. Mater. **24**, 1117 (2014).
- <sup>15</sup>C. Xiang, W. Koo, F. So, H. Sasabe, and J. Kido, Light Sci. Appl. 2, e74 (2013).
- <sup>16</sup>H. S. Jeon, B. Pyo, H. Park, S. R. Park, and M. C. Suh, Org. Electron. Phys. Mater. Appl. 20, 49 (2015).
- <sup>17</sup>S.-J. He and Z.-H. Lu, J. Photonics Energy **6**, 036001 (2016).
- <sup>18</sup>S.-J. He, D.-K. Wang, N. Jiang, J. Zhang, and Z.-H. Lu, Phys. Rev. Appl. 3, 054011 (2015).
- <sup>19</sup>M. N. Berberan-Santos, E. N. Bodunov, and B. Valeur, Chem. Phys. 315, 171 (2005).
- 20 R. M. Amos and W. L. Barnes, Phys. Rev. B 55, 7249 (1997).
- <sup>21</sup>N. Noginova, R. Hussain, M. A. Noginov, J. Vella, and A. Urbas, Optics Express 21, 23087 (2013).
- <sup>22</sup>R. Coehoorn, P. A. Bobbert, and H. Van Eersel, Phys. Rev. B **96**, 184203 (2017).
- 23D. G. Deppe, C. Lei, C. C. Lin, and D. L. Huffaker, J. Mod. Opt. 41, 325 (1994).
- 24C. A. M. Borges, C. A. Rodrigues, R. M. Faria, and F. E. G. Guimarães, Synth. Met. 154, 133 (2005).
- 25 S. Westenhoff, C. Daniel, R. H. Friend, C. Silva, V. Sundström, and A. Yartsev, J. Chem. Phys. 122, 094903 (2005).
- <sup>26</sup>R. Coehoorn and P. A. Bobbert, Phys. Status Solidi A 209, 2354 (2012).
- 27 E. Sacher, J. Electron Spectrosc. Relat. Phenom. 46, 103 (1988).
- <sup>28</sup>H. D. Burrows, M. Fernandes, J. S. De Melo, A. P. Monkman, and S. Navaratnam, J. Am. Chem. Soc. 125, 15310 (2003).
- 29S. Watanabe, A. Furube, and R. Katoh, J. Phys. Chem. A 110(34), 10173 (2006).